5-15-2016

Field-temperature phase diagram and entropy landscape of CeAuSb2

Lishan Zhao
University of St. Andrews

Edward A. Yelland
University of St. Andrews

Jan A. Bruin
University of St. Andrews

Ilya Sheikin
Centre National de la Recherche Scientifique

Paul C. Canfield
Iowa State University, canfield@ameslab.gov

See next page for additional authors

Field-temperature phase diagram and entropy landscape of $CeAuSb_2$

Lishan Zhao,[1,2] Edward A. Yelland,[1,3] Jan A. N. Bruin,[1,4] Ilya Sheikin,[5] Paul C. Canfield,[6] Veronika Fritsch,[7,8] Hideaki Sakai,[1,9] Andrew P. Mackenzie,[1,2,*] and Clifford W. Hicks[2,†]

[1]*Scottish Universities Physics Alliance (SUPA), School of Physics and Astronomy, University of St. Andrews, St. Andrews KY16 9SS, United Kingdom*

[2]*Max Planck Institute for Chemical Physics of Solids, Nöthnitzer Strasse 40, 01187 Dresden, Germany*

[3]*SUPA, School of Physics and Astronomy, and Centre for Science at Extreme Conditions, University of Edinburgh, Mayfield Road, Edinburgh EH9 3JZ, United Kingdom*

[4]*Max Planck Institute for Solid State Research, Heisenbergstrasse 1, 70569 Stuttgart, Germany*

[5]*Laboratoire National des Champs Magnétiques Intenses (LNCMI-EMFL), CNRS, UJF, F-38042 Grenoble, France*

[6]*Ames Laboratory and Department of Physics, Iowa State University, Ames, Iowa 50011, USA*

[7]*Experimental Physics VI, Center for Electronic Correlations and Magnetism, Institute of Physics, University of Augsburg, 86135 Augsburg, Germany*

[8]*Physikalisches Institut, Karlsruhe Institute of Technology, 76131 Karlsruhe, Germany*

[9]*Department of Physics, Osaka University, Toyonaka, Osaka 560-0043, Japan*

(Received 22 February 2016; revised manuscript received 7 April 2016; published 12 May 2016)

We report a field-temperature phase diagram and an entropy map for the heavy-fermion compound $CeAuSb_2$. $CeAuSb_2$ orders antiferromagnetically below $T_N = 6.6$ K and has two metamagnetic transitions, at 2.8 and 5.6 T. The locations of the critical end points of the metamagnetic transitions, which may play a strong role in the putative quantum criticality of $CeAuSb_2$ and related compounds, are identified. The entropy map reveals an apparent entropy balance with Fermi-liquid behavior, implying that above the Néel transition the Ce moments are incorporated into the Fermi liquid. High-field data showing that the magnetic behavior is remarkably anisotropic are also reported.

DOI: 10.1103/PhysRevB.93.195124

I. INTRODUCTION

$CeAuSb_2$ is a heavy-fermion system with the tetragonal $P4/nmm$ structure, moderate electrical anisotropy, and strong magnetic anisotropy [1]. Although it has not been widely studied, it shows strong phenomenological similarities with other cerium-based compounds that have received intense interest. A major theme of study of these systems is to understand and tune the balance between Kondo and Ruderman-Kittel-Kasuya-Yosida (RKKY) interaction: RKKY interaction couples localized spins and favors a magnetically ordered ground state, while strong Kondo interaction quenches local spins and yields a heavy Fermi liquid. Data presented in this paper, and comparison with other compounds, suggest that $CeAuSb_2$ is on the border, with the effects of both Kondo and RKKY interactions apparent in its bulk properties, but neither dominating.

A field-temperature phase diagram, for field along the easy axis (the c axis), of $CeAuSb_2$ is shown in Fig. 1. The indicated phase boundaries are from this work; however, many of its basic features were published in Refs. [2,3]. At zero field, there is a Néel transition at $T_N = 6.6$ K. As the field is increased, there are two first-order metamagnetic transitions, at 2.8 and 5.6 T; at 1.5 K the magnitudes of the metamagnetic jumps are $\approx 0.3\mu_B$/Ce and $0.5\mu_B$/Ce, respectively [2]. The magnetic order terminates at the second metamagnetic transition.

Interestingly, although the magnetism of $CeAuSb_2$ is very different from that of the isostructural compound $CeAgSb_2$, it is similar to that of a range of less obviously related compounds. $CeAuSb_2$ is an antiferromagnetic with easy-axis anisotropy, while $CeAgSb_2$ has a net ferromagnetic moment, and easy-plane anisotropy [4]. In contrast, the compounds $CeNiGe_3$ [5,6], $CeRh_2Si_2$ [7,8], and $YbNiSi_3$ [9,10], and the $CeRu_2Si_2$-based compounds $(Ce_{0.8}La_{0.2})Ru_2Si_2$ [11–13], $CeRu_2(Si_{0.9}Ge_{0.1})_2$ [14,15], and $Ce(Ru_{0.092}Rh_{0.08})_2Si_2$ [16,17] are all easy-axis compounds, like $CeAuSb_2$. All are antiferromagnets. All of them, like $CeAuSb_2$, show two metamagnetic transitions when the field is directed along the easy axis, and with the exception of $Ce(Ru_{0.92}Rh_{0.08})_2Si_2$ the magnetic order of each terminates at the second metamagnetic transition. χ_c/χ_a of $CeAuSb_2$ is 17 just above T_N [1]; of $CeRh_2Si_2$, 5 just above its Néel temperature [18]; and of $CeRu_2Si_2$, 15 at 10 K [19]. $CeNiGe_3$ is an orthorhombic system where the a axis is the easy axis; χ_a/χ_b and χ_a/χ_c are 11 and 17, respectively, just above its T_N [5].

Therefore, study of $CeAuSb_2$ is likely to have bearing on a range of other compounds. Comparison with the $CeRu_2Si_2$-based compounds is of particular interest because of the amount known about that system. $CeRu_2Si_2$ itself has a Kondo temperature T_K of $\sim$24 K [19], and strong antiferromagnetic fluctuations at low temperature, but no static order [20]; the Kondo effect appears to win out over the RKKY interaction by a small margin. Substitution can alter the balance: partial substitution of La for Ce, e.g., decreases T_K and induces the static antiferromagnetic order mentioned above [13,21,22]. The substitution applies an effective negative pressure: the

*mackenzie@cpfs.mpg.de
†hicks@cpfs.mpg.de

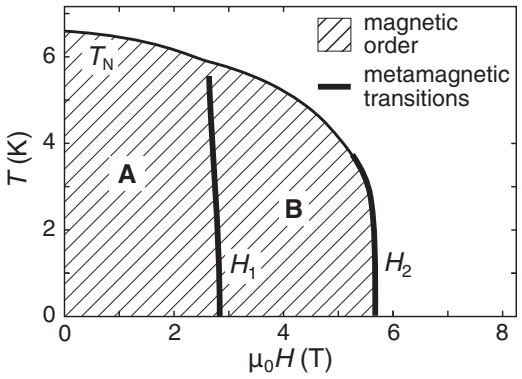

FIG. 1. Field-temperature phase diagram of $CeAuSb_2$, for the field **H** along the easy magnetic axis. T_N is the Néel temperature, and H_1 and H_2 are the metamagnetic transition fields. The indicated phase boundaries are from this work.

lattice is expanded, and when it is compressed again with (positive) hydrostatic pressure the antiferromagnetism is suppressed [23]. The similarity between the phase diagrams of $CeAuSb_2$ and substituted $CeRu_2Si_2$-based compounds suggests that $CeAuSb_2$ acts, broadly, as a negative-pressure version of $CeRu_2Si_2$. Usefully, it is a version without intrinsic substitution disorder or, with reference to $Ce_{1-x}La_xRu_2Si_2$, dilution of Ce spins. It may allow RKKY-Kondo crossover to be studied with positive rather than negative pressure.

The main aim of the present work is to refine the phase diagram of $CeAuSb_2$. The metamagnetic transitions are thought to be first order, but clear hysteresis has not been seen and their critical end points have not been precisely located [2]. As elaborated upon in Sec. VI, the end points may prove crucial to possible quantum criticality in $CeAuSb_2$ and related compounds. In addition to locating the critical end points of $CeAuSb_2$, we also report an entropy map across the field-temperature phase diagram, which yields both similarities and notable contrasts with the above compounds.

II. CRYSTAL GROWTH

Single $CeAuSb_2$ crystals were grown by a self-flux method, similar to that described in Refs. [24,25]. High-purity ingots of Ce (99.99%, Ames Laboratory), Au (99.999%, Alfa Aesar), and Sb (99.999%, Alfa Aesar) were placed in an alumina crucible with a Ce:Au:Sb atomic ratio of 1:6:12. The crucible was then sealed in an evacuated quartz ampoule and heated to 1100°C for 10 h, followed by cooling to 700° over a period of 100 h. The excess flux was decanted with a centrifuge at 700°C. Measurement by energy-dispersive x-ray spectroscopy (EDX) confirmed that the crystals are stoichiometric to within the 5% measurement precision. The residual resistivity ratios of the crystals used in this work were between 6 and 9. A photograph of an as-grown $CeAuSb_2$ crystal is shown in Fig. 2.

III. RESULTS: RESISTIVITY

For measurement of resistivity, samples were cut into narrow bars with a wire saw. The as-grown samples were naturally thin along the c axis, so polishing to reduce thickness was not necessary. The samples were measured with a typical

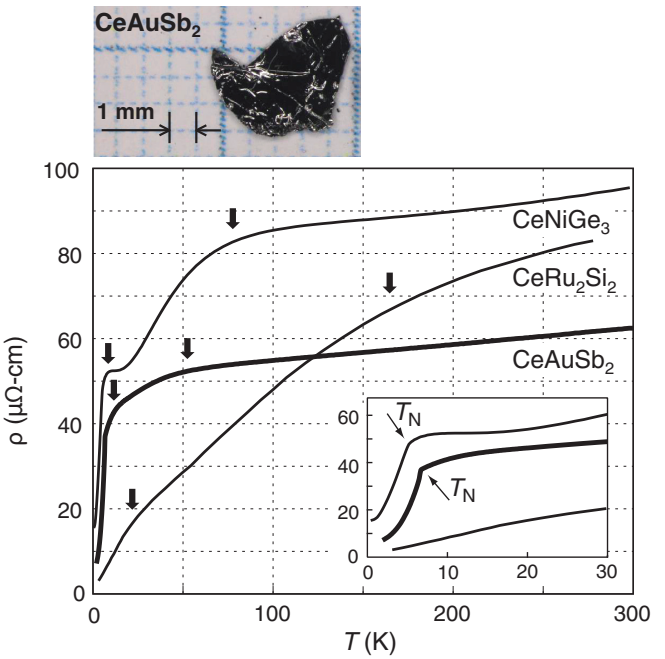

FIG. 2. Top: a photograph of an as-grown crystal of $CeAuSb_2$. Bottom: comparison of $\rho(T)$ of $CeNiGe_3$ [5], $CeRu_2Si_2$ [19], and $CeAuSb_2$ (this work). For $CeRu_2Si_2$ and $CeAuSb_2$, the current **I** is in the plane, and for $CeNiGe_3$, an orthorhombic material, $\mathbf{I} \parallel \hat{\mathbf{c}}$. The arrows mark broad shoulders, discussed in the text.

four-terminal method using a lock-in amplifier, with typically a 100-μA excitation current at a frequency on the order of 100 Hz. Contacts to the sample were made with DuPont 6838 silver paste, baked at 180°C for 2.5 h.

We start in Fig. 2 with a comparison of the resistivities $\rho(T)$ of $CeAuSb_2$, $CeRu_2Si_2$, and $CeNiGe_3$. The room-temperature values are similar; respective comparison of $CeAuSb_2$ with $LaAuSb_2$ [26] and $CeRu_2Si_2$ with $LaRu_2Si_2$ [19] show that at room temperature, where defect scattering gives only a small portion of the resistivity, scattering from cerium spins accounts for roughly half the resistivity, and a greater portion as T is reduced. The resistivities also all show two broad shoulders, marked by the arrows in Fig. 2. The higher-temperature shoulders are due to thermal occupation of excited crystal electric field states. The origin of the lower-temperature shoulders may differ from compound to compound; in $CeRu_2Si_2$ it is attributed to the Kondo effect [19]. In both $CeNiGe_3$ and $CeAuSb_2$ the shoulder is at a lower temperature than in $CeRu_2Si_2$; both these compounds also show Néel order, so the lower-temperature shoulder could be due to onset of short-range magnetic order at $T > T_N$, or the Kondo effect, or a combination.

Low-temperature measurements of the resistivity of $CeAuSb_2$ were done on two samples from the same growth batch, with cross sections $\approx 180 \times 130$ and $\approx 250 \times 150\,\mu$m (the shorter dimension along the c axis). They were measured together in an adiabatic demagnetization refrigerator. Figure 3 shows the resistivity against field of one sample at various fixed temperatures. At the lowest temperatures, ρ increases sharply at the first metamagnetic transition (at applied field H_1) and decreases sharply at the second (H_2). Elevated resistivity

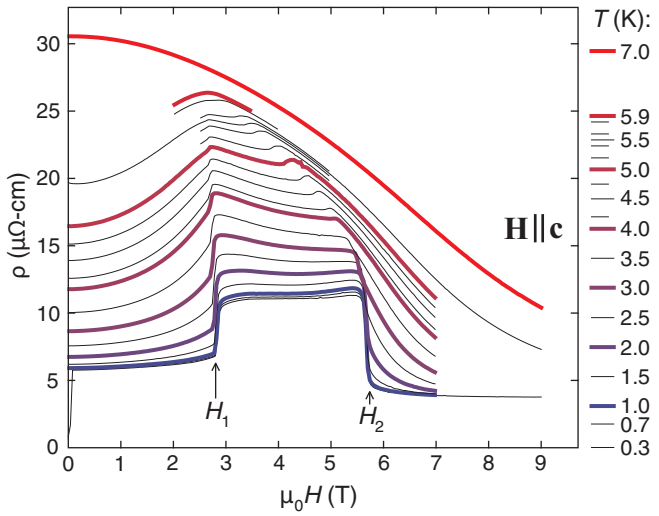

FIG. 3. In-plane resistivity of $CeAuSb_2$ against magnetic field, applied along the c axis. The plotted data are from increasing-field ramps. The sharp drop in resistivity at the lowest field and temperature is probably due to superconductivity of $AuSb_2$ on the surface [27]; it can be removed by polishing.

between H_1 and H_2 is also seen in $CeNiGe_3$ [5], $YbNiSi_3$ [9], and $CeRh_2Si_2$ [7].

Data from increasing-field and decreasing-field ramps are shown together in Fig. 4; magnet hysteresis is excluded by measuring the field with a Hall sensor placed near the sample. Hysteresis in the metamagnetic transition fields shows that the transitions are first order. The magnitude of the hysteresis against temperature is shown in Fig. 4(b): it decreases steadily as the temperature is increased (proving that it is not an artifact of instrument hysteresis), disappearing within experimental resolution above ∼5 K for the first and above ∼3 K for the second transition.

Rounding of the transitions and residual instrument hysteresis make it impossible to pinpoint the temperatures where the hysteresis ends. To locate the end points more precisely,

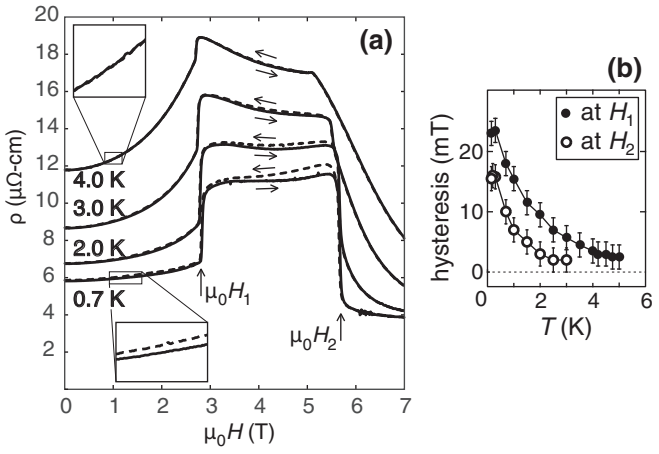

FIG. 4. (a) Data from increasing- and decreasing-field ramps, plotted together. (b) Difference in the transition fields between the increasing- and decreasing-field ramps, plotted against temperature. For all temperatures, the ramp rate was 0.1 T/min.

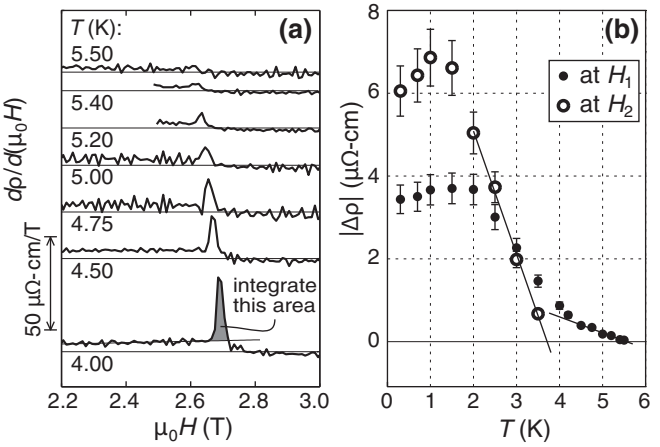

FIG. 5. (a) $d\rho/d(\mu_0 H)$ against $\mu_0 H$ at the first transition, at temperatures approaching the critical end point. On the bottom curve, the method for determining the resistivity jump $\Delta\rho$ is illustrated: a background is fit to the data to the left (right) of the peak for the first (second) metamagnetic transition, and the peak integrated. (b) $|\Delta\rho|$ against temperature.

we analyzed the magnitudes of the resistivity jumps, $|\Delta\rho|$, determined by integrating the peaks in the derivative $d\rho/d(\mu_0 H)$ as illustrated in Fig. 5(a). Rounding introduces moderate systematic error, but by following the same procedure at each temperature, random error is minimized. $|\Delta\rho|$ against T is shown in Fig. 5(b); the error bars are the estimated systematic error. Linear fits through the higher-temperature points locate the end points of the first and second transitions at 5.6 and 3.7 K, respectively.

In Fig. 4, hysteresis is apparent not only in the transition fields, but also in the magnitude of the resistivity across the magnetically ordered region: ρ is larger on decreasing- than on increasing-field ramps. Hysteresis between H_1 and H_2 has been reported before [2,3]; its origin is not resolved, although antiferromagnetic domain walls are a natural possibility. We add two further observations:

(1) There is hysteresis below H_1, as well as between H_1 and H_2.

(2) The magnitude of the hysteresis decreases approximately linearly as the temperature is increased, disappearing between 4 and 5 K.

IV. RESULTS: SPECIFIC HEAT CAPACITY

The specific heat capacity C of a sample roughly 2 mm across and 0.1 mm thick, with mass 4.0 mg, was measured in a Quantum Design Physical Properties Measurement System. The relaxation time method was used: at each point the sample temperature was raised by 2%, then the relaxation time was measured.

C/T against temperature at selected magnetic fields is plotted in Fig. 6. C/T of $LaAuSb_2$, from Ref. [2], is also shown, as an estimate of the nonmagnetic contribution; up to at least ∼7 K it is much smaller than C/T of $CeAuSb_2$. The dominant feature in the low-temperature heat capacity of $CeAuSb_2$ is the Néel transition. At low fields, the peak at T_N is relatively narrow. It is broader in the vicinity of the first

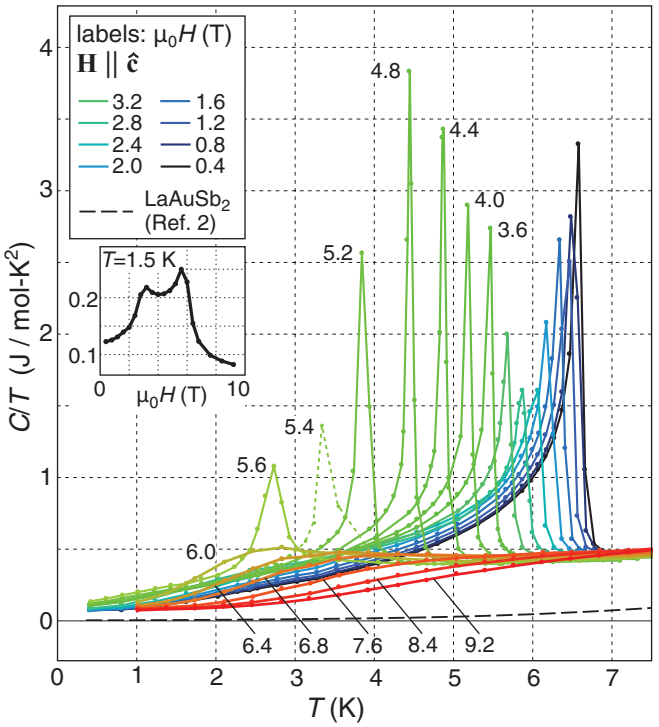

FIG. 6. C/T of $CeAuSb_2$ at selected fields. Inset: C/T against field at $T = 1.5$ K.

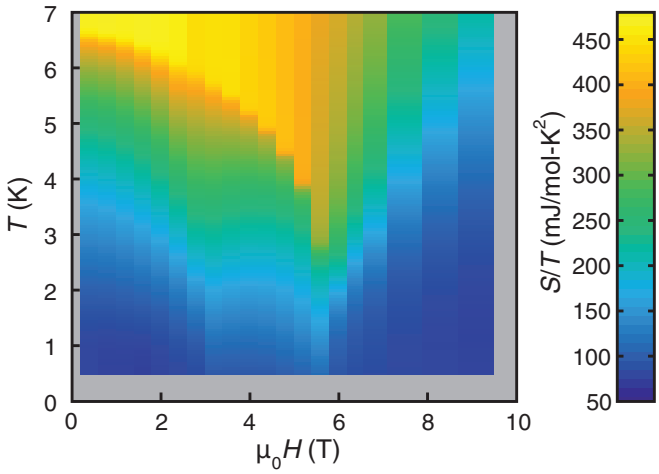

FIG. 7. Entropy over temperature of $CeAuSb_2$ against temperature and c-axis magnetic field.

critical end point, at 2.6 T and 5.6 K, and becomes very sharp as the field is increased towards the second critical end point, at 5.2 T and 3.7 K.

The inset in Fig. 6 shows C/T against field at $T = 1.5$ K. It is higher between H_1 and H_2 than on either side. This behavior has also been established for $CeNiGe_3$ [5], $Ce(Ru_{0.92}Rh_{0.08})_2Si_2$ [17], and (though less pronounced) $Ce_{0.9}La_{0.1}Ru_2Si_2$ [12].

C/T may be integrated from 0 K at each field to yield the entropy, S. To do so, an extrapolation to 0 K is required, although the data extend to low enough temperature that the precise form of the extrapolation is not critical. We take, at each field, a linear extrapolation from the lowest-temperature data point to 79.5 mJ/(mol K^2) at 0 K, which is an apparent base value in the data. A map of the resulting entropy, divided by temperature, is shown in Fig. 7. Below the Néel transition, the entropy is generally higher over the field range $H_1 < H < H_2$ than on either side.

At lower fields, S/T and C/T closely match above T_N: at $\mu_0 H = 0.4$ T and $T = 7$ K, S/T and C/T are 0.47 and 0.48 J/(mol K^2), respectively. In other words, the magnetic order maintains entropy balance with a Fermi-liquid-like, T-independent C/T. (Subtracting C/T of $LaAuSb_2$, as an estimate for the phonon contribution, makes little difference: S/T and C/T are respectively revised to 0.45 and 0.41 J/(mol K^2).) Entropy balance with a Fermi liquid suggests that the Ce $4f$ moments are fully incorporated into the Fermi liquid below some temperature that exceeds T_N, such that in the absence of magnetic order C/T would be T independent down to 0 K. This behavior is in contrast to $CeNiGe_3$, $YbNiSi_3$, and $Ce_{0.7}La_{0.3}Ru_2Si_2$. Based on analysis of published data [5,9,28], and taking reasonable extrapolations of C/T to 0 K, we find that in these compounds S/T at 7 K (above T_N for each) exceeds C/T by more than a factor of 2. (Specifically, S/T and C/T at 7 K are respectively 0.65 and 0.30 J/(mol K^2) for $CeNiGe_3$, ≈ 0.63 and 0.27 J/(mol K^2) for $YbNiSi_3$, and $\approx$0.58 and 0.21 J/(mol K^2) for $Ce_{0.7}La_{0.3}Ru_2Si_2$.) In these compounds the $4f$ moments appear to give a quasi-independent contribution to S/T that is in addition to a Fermi-liquid contribution: the moments are strongly disordered by $T \sim 7$ K, making a large contribution to the total entropy, but at 7 K the dominant contribution to C/T is from the Fermi liquid.

It is also notable that above T_N, C/T of $CeAuSb_2$ drops very quickly to its Fermi-liquid value, whereas C/T of each of $CeNiGe_3$, $YbNiSi_3$, and $Ce_{0.7}La_{0.3}Ru_2Si_2$ has a strong decaying tail that extends at least a few kelvin above T_N. Such tails are common in local-moment systems, e.g., in $PdCrO_2$ [29], and arise from gradual onset of short-range magnetic order above T_N. They provide further evidence that in these compounds the $4f$ moments and Fermi liquid are quasi-independent systems, while in $CeAuSb_2$ they are not.

At low fields, the entropy of $CeAuSb_2$ above T_N is a substantial fraction of $R \ln 2$: at 0.4 T and 7 K, $S = 3.3$ J/(mol K) $= 0.57 R \ln 2$. The $T > T_N$ entropy is gradually suppressed as the field is increased; indicating that the heavy-fermion state is gradually suppressed through polarization of the Ce moments.

V. RESULTS: HIGH-FIELD MEASUREMENTS

To probe the magnetic anisotropy, resistivity and torque magnetometry measurements up to 35 T were performed at the Laboratoire National des Champs Magnétiques Intenses in Grenoble, France. The samples were mounted on a rotatable platform, to vary the field angle. The transport sample was a bar with cross-sectional area 230×90 μm^2. The dimensions of the torque magnetometry sample were $\sim 250 \times 250 \times 50$ μm^3. Results are shown in Fig. 8.

Previously published measurements showed that T_N is almost independent of in-plane field up to 18 T [2]. Our measurements show similarly that the metamagnetic transition fields are remarkably unaffected by the presence of a strong

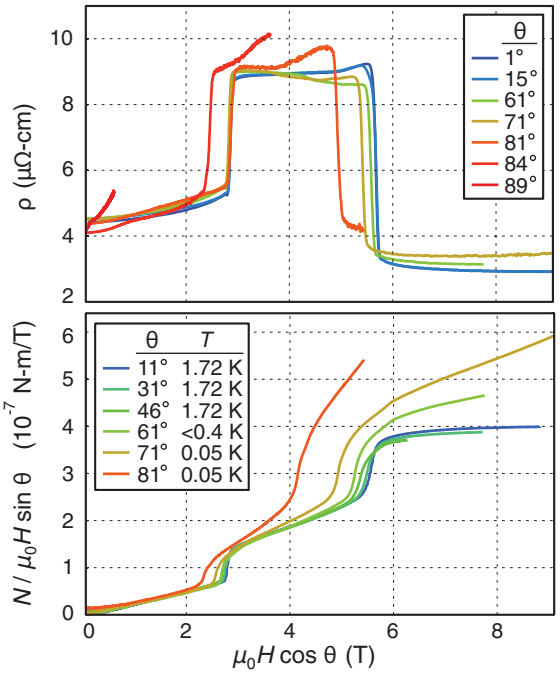

FIG. 8. Measurements of $CeAuSb_2$ in fields up to 35 T. θ is the angle between **H** and the c axis. Top: resistivity against c-axis field $\mu_0 H\cos(\theta)$. Bottom: torque N, divided by the in-plane component of the field, against $\mu_0 H\cos(\theta)$. Measurements at 1.72 K were performed at St. Andrews, and at lower temperatures in the high-field laboratory in Grenoble.

in-plane field. In the figure, ρ is plotted against the c-axis field, $H_{\hat{\mathbf{c}}} = H\cos\theta$, with θ the angle between **H** and the c axis. The form of $\rho(H_{\hat{\mathbf{c}}})$ changes little as the in-plane field is increased, even to the point that **H** is only a few degrees out of the plane.

The metamagnetic transitions are also apparent in the torque data. Plotted in the bottom panel of Fig. 8 is the torque N divided by the in-plane field $H\sin\theta$: if the field-induced magnetization is pinned to the c axis, and is a function of $H_{\hat{\mathbf{c}}}$ alone (i.e., independent of the in-plane field), then the graph of $N/H\sin\theta$ against $H_{\hat{\mathbf{c}}}$ will be independent of field angle. The data show that this is essentially the case for $CeAuSb_2$ up to $\theta \sim 70°$, confirming that the magnetism of $CeAuSb_2$ is strongly easy-axis type. As the field gets very close to the ab plane, the metamagnetic transitions move to lower $H_{\hat{\mathbf{c}}}$.

VI. PHASE DIAGRAM AND DISCUSSION

Figure 9 shows the field-temperature phase diagram derived from the resistivity and specific heat data presented above. The first-order metamagnetic transition lines, and their critical end points, are indicated. The first metamagnetic line separates regions of magnetic order that may be designated the A and B phases. The line slopes leftward as T is raised, consistent with the observation that the B phase has higher entropy than the A phase. In contrast to a previous report, we do not find evidence for an intermediate phase along either metamagnetic line [3].

The first critical end point, at a temperature of 5.6 K, appears to lie ≈0.4 K below T_N at that field, although the present data do not allow this to be concluded with high certainty. It would be useful to investigate the metamagnetism further,

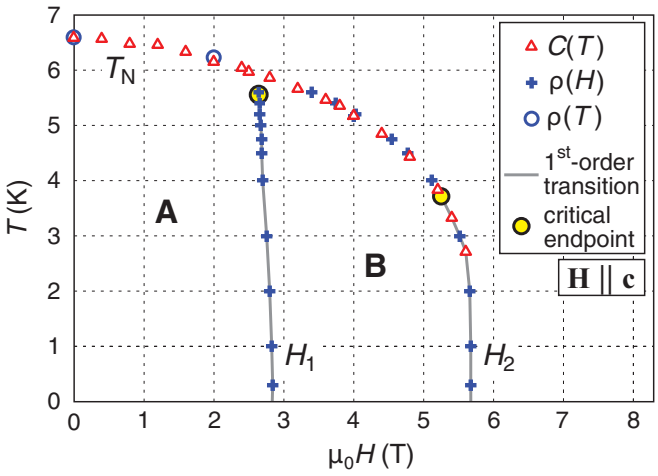

FIG. 9. Phase diagram of $CeAuSb_2$, derived from measurements of ρ against H, ρ against T, and specific heat against T.

for example through ac susceptibility measurements [30]. If the end point is indeed below T_N, it would be interesting to determine whether the boundary between the A and B phases continues to T_N as a crossover or a second-order transition; the former implies adiabatic continuity between the two phases, and the latter an additional symmetry breaking.

Quantum criticality is a major theme in the study of heavy-fermion systems, and in studies of criticality the location of critical end points is vital knowledge. For example, many key properties of $CeRu_2Si_2$ are explainable by a missed quantum critical end point at $\mu_0 H \approx 7.6$ T [31]. At the field-driven antiferromagnetic quantum critical point of $YbRh_2Si_2$, it has been proposed that it is in fact close proximity of a metamagnetic critical end point and an antiferromagnetic quantum critical point (QCP), rather than the antiferromagnetic QCP alone, that drives the observed divergences in the Sommerfeld coefficient and magnetic susceptibility [32–34]. The superconductivity of URhGe [35] and the anomalous phase in $Sr_3Ru_2O_7$ [30] both form around low-temperature metamagnetic critical end points.

In $CeAuSb_2$, the second critical end point is at a temperature of 3.7 K. This is more than half the maximum T_N, so quantum critical scaling to $T \sim 0$ K is not expected. However, it would be a very compelling experiment to track the end points with pressure, and to attempt to drive them to 0 K. (This may also be achievable with very high in-plane field: the data in Fig. 8 show some reduction of the c-axis transition fields with 30-T-scale in-plane fields.) The antiferromagnetic order of both $CeRh_2Si_2$ and $CeNiGe_3$ can be suppressed with pressure, with superconductivity appearing in a window of pressure around the antiferromagnetic QCP [36,37]. It would be interesting to determine whether metamagnetic quantum criticality is also involved in this superconductivity. Regarding $CeAuSb_2$, a published pressure study at $H = 0$ showed that pressure initially increases the temperature of the first resistivity shoulder and decreases T_N [26].

As described above, entropy balance with a Fermi liquid suggests that Kondo coupling is important in $CeAuSb_2$, incorporating the $4f$ moments into the Fermi liquid by some temperature that exceeds T_N; strong Kondo coupling probably

sets in at the temperature of the first resistivity shoulder, at ∼12 K. Phenomenologically, $CeAuSb_2$ therefore appears to be intermediate to $CeRu_2Si_2$, where Kondo coupling is strong enough that static magnetic order never emerges, and, e.g., $CeNiGe_3$ and $Ce_{0.7}La_{0.3}Ru_2Si_2$, where the moments and conduction electrons appear to be quasidecoupled at all temperatures.

We also note a strong similarity between the phenomenology of $CeAuSb_2$ and $Sr_3Ru_2O_7$, which was in fact the original motivation for this study of $CeAuSb_2$: both show strongly enhanced resistivity over a finite window of field (in the case of $Sr_3Ru_2O_7$, between ≈7.9 and 8.1 T), bounded by first-order metamagnetic transitions, and over which the entropy is also higher [30,38]. $Sr_3Ru_2O_7$ is very clearly an itinerant system, while in $CeAuSb_2$ the moments probably have strong local character below T_N. The similar behavior in spite of this major qualitative difference suggests a deep link between the two systems.

VII. CONCLUSION

In conclusion, we have produced a refined field-temperature phase diagram of $CeAuSb_2$, and an entropy map spanning the region of magnetic order. We have also highlighted similarities between $CeAuSb_2$ and other compounds. The observed metamagnetic transitions were sufficiently sharp to resolve clear hysteresis and to locate their critical end points, showing that $CeAuSb_2$ can now be grown with sufficiently low disorder to make it a useful reference material and target for further study.

ACKNOWLEDGMENTS

We acknowledge useful discussion with Manuel Brando and Christoph Geibel. We thank Hanoh Lee for advice on crystal growth. We thank the EPSRC (Grants No. EP/1031014/1 and No. EP/G03673X/1) and the Max Planck Society for financial support. We also acknowledge the support of the LNCMI-CNRS, member of the European Magnetic Field Laboratory (EMFL). E.A.Y. acknowledges support from the Royal Society. P.C.C. was supported, in part, by the U.S. Department of Energy, Office of Basic Energy Science, Division of Materials Sciences and Engineering through the Ames Laboratory. Ames Laboratory is operated for the U.S. Department of Energy by Iowa State University under Contract No. DE-AC02-07CH11358. V.F. acknowledges support by the Deutsche Forschungsgemeinschaft through FOR Grant No. 960. H.S. gratefully acknowledges fellowships from the Canon Foundation.

The raw data for the figures in this article can be found in Ref. [39].

[1] A. Thamizhavel, T. Takeuchi, T. Okubo, M. Yamada, R. Asai, S. Kirita, A. Galatanu, E. Yamamoto, T. Ebihara, Y. Inada, R. Settai, and Y. Onuki, Anisotropic electrical and magnetic properties of Ce TSb_2 (T = Cu, Au, and Ni), single crystals, Phys. Rev. B **68**, 054427 (2003).

[2] L. Balicas, S. Nakatsuji, H. Lee, P. Schlottmann, T. P. Murphy, and Z. Fisk, Magnetic field-tuned quantum critical point in $CeAuSb_2$, Phys. Rev. B **72**, 064422 (2005).

[3] K.-A. Lorenzer, A. M. Strydom, A. Thamizhavel, and S. Paschen, Temperature-field phase diagram of quantum critical $CeAuSb_2$, Phys. Status Solidi B **250**, 464 (2013).

[4] E. Jobiliong, J. S. Brooks, E. S. Choi, H. Lee, and Z. Fisk, Magnetization and electrical-transport investigation of the dense Kondo system $CeAgSb_2$, Phys. Rev. B **72**, 104428 (2005).

[5] E. D. Mun, S. L. Bud'ko, A. Kreyssig, and P. C. Canfield, Tuning low-temperature physical properties of $CeNiGe_3$ by magnetic field, Phys. Rev. B **82**, 054424 (2010).

[6] A. P. Pikul, D. Kaczorowski, T. Plackowski, A. Czopnik, H. Michor, E. Bauer, G. Hilscher, P. Rogl, and Yu. Grin, Kondo behavior in antiferromagnetic $CeNiGe_3$, Phys. Rev. B **67**, 224417 (2003).

[7] W. Knafo, D. Aoki, D. Vignolles, B. Vignolle, Y. Klein, C. Jaudet, A. Villaume, C. Proust, and J. Flouquet, High-field metamagnetism in the antiferromagnet $CeRh_2Si_2$, Phys. Rev. B **81**, 094403 (2010).

[8] A. Palacio Morales, A. Pourret, G. Seyfarth, M. T. Suzuki, D. Braithwaite, G. Knebel, D. Aoki, and J. Flouquet, Fermi surface instabilities in $CeRh_2Si_2$ at high magnetic field and pressure, Phys. Rev. B **91**, 245129 (2015).

[9] S. L. Bud'ko, P. C. Canfield, M. A. Avila, and T. Takabatake, Magnetic-field tuning of the low-temperature state of $YbNiSi_3$, Phys. Rev. B **75**, 094433 (2007).

[10] M. A. Avila, M. Sera, and T. Takabatake, $YbNiSi_3$: An antiferromagnetic Kondo lattice with strong exchange interaction, Phys. Rev. B **70**, 100409(R) (2004).

[11] J.-M. Mignot, J.-L. Jacoud, L.-P. Regnault, J. Rossat-Mignod, P. Haen, P. Lejay, Ph. Boutrouille, B. Hennion, and D. Petitgrand, Neutron diffraction study of (Ce, La)Ru_2Si_2 alloys in an external field, Physica B **163**, 611 (1990).

[12] D. Aoki, C. Paulsen, T. D. Matsuda, L. Malone, G. Knebel, P. Haen, P. Lejay, R. Settai, Y. Ōnuki, and J. Flouquet, Pressure evolution of the magnetic field induced ferromagnetic fluctuations through the pseudo-metamagnetism of $CeRu_2Si_2$, J. Phys. Soc. Jpn. **80**, 053702 (2011).

[13] Y. Shimizu, Y. Matsumoto, K. Aoki, N. Kimura, and H. Aoki, Anomalous transport properties via the competition between the RKKY interaction and the Kondo effect in $Ce_xLa_{1-x}Ru_2Si_2$, J. Phys. Soc. Jpn. **81**, 044707 (2012).

[14] J. M. Mignot, L. P. Regnault, J. L. Jacoud, J. Rossat-Mignod, P. Haen, and P. Lejay, Incommensurabilities and metamagnetism in the heavy-fermion alloys $(Ce_{0.8}La_{0.1})Ru_2Si_2$ and $CeRu_2(Si_{0.9}Ge_{0.1})_2$, Physica B **171**, 357 (1991).

[15] M. Sugi, Y. Matsumoto, N. Kimura, T. Komatsubara, H. Aoki, T. Terashima, and S. Uji, Fermi Surface Properties of

$CeRu_2(Si_{1-x}Ge_x)_2$ in Magnetic Fields Above the Metamagnetic Transitions, Phys. Rev. Lett. **101**, 056401 (2008).

[16] C. Sekine, T. Sakakibara, H. Amitsuka, Y. Miyako, and T. Goto, Magnetic properties and phase diagram of $Ce(Ru_{1-x}Rh_x)_2Si_2$ ($0 \leqslant x < 0.5$), J. Phys. Soc. Jpn. **61**, 4536 (1992).

[17] D. Aoki, C. Paulsen, H. Kotegawa, F. Hardy, C. Meingast, P. Haen, M. Boukahil, W. Knafo, E. Ressouche, S. Raymond, and J. Flouquet, Decoupling between field-instabilities of antiferromagnetism and psuedo-metamagnetism in Rh-doped $CeRu_2Si_2$ Kondo lattice, J. Phys. Soc. Jpn. **81**, 034711 (2012).

[18] R. Settai, A. Misawa, S. Araki, M. Kosaki, K. Sugiyama, T. Takeuchi, K. Kindo, Y. Haga, E. Yamamoto, and Y. Ōnuki, Single crystal growth and magnetic properties of $CeRh_2Si_2$, J. Phys. Soc. Jpn. **66**, 2260 (1997).

[19] P. Haen, J. Flouquet, F. Lapierre, P. Lejay, and G. Remenyi, Metamagnetic-like transition in $CeRu_2Si_2$?, J. Low Temp. Phys. **67**, 391 (1987).

[20] S. Raymond, L. P. Regnault, S. Kambe, J. Flouquet, and P. Lejay, Switching of the magnetic interactions from antiferromagnetic to ferromagnetic in the heavy-fermion compound $CeRu_2Si_2$ under high magnetic field, J. Phys. Condens. Matter **10**, 2363 (1998).

[21] A. Amato, D. Jaccard, J. Sierro, P. Haen, P. Lejay, and J. Flouquet, Transport properties under magnetic fields of the heavy fermion system $CeRu_2Si_2$ and related compounds (Ce, La)Ru_2Si_2, J. Low Temp. Phys. **77**, 195 (1989).

[22] W. Knafo, S. Raymond, P. Lejay, and J. Flouquet, Antiferromagnetic criticality at a heavy-fermion quantum phase transition, Nat. Phys. **5**, 753 (2009).

[23] P. Haen, F. Lapierre, J. Voiron, and J. Flouquet, Vanishing of magnetic order in $Ce_{0.8}La_{0.2}Ru_2Si_2$ under pressure, J. Phys. Soc. Jpn. **65**, 27 (1996).

[24] P. C. Canfield and Z. Fisk, Growth of single-crystals from metallic fluxes, Philos. Mag. B **65**, 1117 (1992).

[25] P. C. Canfield and I. R. Fisher, High-temperature solution growth of intermetallic single crystals and quasicrystals, J. Cryst. Growth **225**, 155 (2001).

[26] S. Seo, V. A. Sidorov, H. Lee, D. Jang, Z. Fisk, J. D. Thompson, and T. Park, Pressure effects on the heavy-fermion antiferromagnet $CeAuSb_2$, Phys. Rev. B **85**, 205145 (2012).

[27] B. T. Matthias, T. H. Geballe, and V. B. Compton, Superconductivity, Rev. Mod. Phys. **35**, 1 (1963).

[28] M. J. Besnus, P. Lehmann, and A. Meyer, Heat capacity study of the (La-Ce)Ru_2Si_2 and (Ce-Y)Ru_2Si_2 Kondo systems, J. Magn. Magn. Mater. **63–64**, 323 (1987).

[29] H. Takatsu, H. Yoshizawa, S. Yonezawa, and Y. Maeno, Critical behavior of the metallic triangular-lattice Heisenberg antiferromagnet $PdCrO_2$, Phys. Rev. B **79**, 104424 (2009).

[30] S. A. Grigera, P. Gegenwart, R. A. Borzi, F. Weickert, A. J. Schofield, R. S. Perry, T. Tayama, T. Sakakibara, Y. Maeno, A. G. Green, and A. P. Mackenzie, Disorder-sensitive phase formation linked to metamagnetic quantum criticality, Science **306**, 1154 (2004).

[31] F. Weickert, M. Brando, F. Steglich, P. Gegenwart, and M. Garst, Universal signatures of the metamagnetic quantum critical endpoint: Application to $CeRu_2Si_2$, Phys. Rev. B **81**, 134438 (2010).

[32] T. Misawa, Y. Yamaji, and M. Imada, $YbRh_2Si_2$: Quantum tricritical behavior in itinerant electron system, J. Phys. Soc. Jpn. **77**, 093712 (2008).

[33] A. Hackl and M. Vojta, Zeeman-Driven Lifshitz Transition: A Model for the Experimentally Observed Fermi-Surface Reconstruction in $YbRh_2Si_2$, Phys. Rev. Lett. **106**, 137002 (2011).

[34] P. Gegenwart, J. Custers, Y. Tokiwa, C. Geibel, and F. Steglich, Ferromagnetic Quantum Critical Fluctuations in $YbRh_2(Si_{0.95}Ge_{0.05})_2$, Phys. Rev. Lett. **94**, 076402 (2005).

[35] E. A. Yelland, J. M. Barraclough, W. Wang, K. V. Kamenev, and A. D. Huxley, High-field superconductivity at an electronic topological transition in URhGe, Nat. Phys. **7**, 890 (2011).

[36] H. Kotegawa, K. Takeda, T. Miyoshi, S. Fukushima, H. Hidaka, T. C. Kobayashi, T. Akazawa, Y. Ohishi, M. Nakashima, A. Thamizhavel, R. Settai, and Y. Ōnuki, Pressure-induced superconductivity emerging from antiferromagnetic phase in $CeNiGe_3$, J. Phys. Soc. Jpn. **75**, 044713 (2006).

[37] S. Araki, M. Nakashima, R. Settai, T. C. Kobayashi, and Y. Ōnuki, Pressure-induced superconductivity in an antiferromagnet $CeRh_2Si_2$, J. Phys. Condens. Matter **14**, L377 (2002).

[38] A. W. Rost, R. S. Perry, J.-F. Mercure, A. P. Mackenzie, and S. A. Grigera, Entropy landscape of phase formation associated with quantum criticality in $Sr_3Ru_2O_7$, Science **325**, 1360 (2009).

[39] http://dx.doi.org/10.17630/fba45bfc-281b-44f4-9db8-a2786613851c.